Developments of Low-Cost Aqueous Sodium-Ion Batteries with Prussian Blue Analogue Positive Electrodes for Solar Energy Storage Applications

Summary of Work (5000 Words)

for

The award of Doctor of Philosophy in Science (Chemistry)

by

Pappu Naskar

Registration No.: R-18RS205120193

Date of Registration: 9th January, 2021

Department of Chemistry, Presidency University

Kolkata 700073, India

January, 2024

Contents

Abbreviations		1
Chapter 1:	Fundamental Aspects of Aqueous Sodium-Ion Batteries for Solar Energy Storage	2-5
Chapter 2:	Aqueous Sodium-Ion Hybrid Batteries with $Na_2NiFe(CN)_6$ Prussian Blue Analogue Positive and Functionalized Carbons Negative Electrodes in Starved Electrolyte Configuration	6-8
Chapter 3:	Aqueous Sodium-Ion Batteries with $Na_2CoFe(CN)_6$ Prussian Blue Analogue Positive and Sodium Vanadate Negative Negative Electrodes in Silica Gel Electrolyte	9-11
Chapter 4:	Aqueous Sodium-Ion Hybrid Batteries with $Na_2MnFe(CN)_6$ Prussian Blue Analogue Positive and Ferric Oxide Negative Electrodes in Silica Gel Electrolyte	12-14
Chapter 5:	Aqueous Sodium-Ion Hybrid Batteries with $Na_2Mn_{0.5}Ni_{0.5}Fe(CN)_6$ Prussian Blue Analogue Positive and Na-Doped Ferric Oxide Negative Electrodes in Carboxymethyl Cellulose-Silica Gel Electrolyte	15-17
Chapter 6:	Aqueous Sodium-Ion Batteries with $Na_2Co_{0.5}Ni_{0.5}Fe(CN)_6$ Prussian Blue Analogue Positive and Sodium Titanium Phosphate Negative Electrodes in Silica Gel Electrolyte	18-20
Chapter 7:	Aqueous Sodium-Ion Batteries with $Na_2Ni_{0.33}Co_{0.33}Mn_{0.33}Fe(CN)_6$ Prussian Blue Analogue Positive and Hydrogen Vanadate Negative Electrodes in Carboxymethyl Cellulose-Silica Gel Electrolyte	21-23
Chapter 8:	Aqueous Sodium-Ion Batteries with High-Entropy $Na_2Mn_{0.2}Fe_{0.2}Co_{0.2}Ni_{0.2}Cu_{0.2}Fe(CN)_6$ Prussian Blue Analogue Positive and $Na_2CuFe(CN)_6$-Derived Oxide Negative Electrodes in Carboxymethyl Cellulose-Silica Gel Electrolyte	24-26
List of Publications		27
List of Conference Attended		28

Abbreviations

Abbreviation	Meaning
EDLCs	Electrical double-layer capacitors
CV	Cyclic voltammetric
PB	Prussian blue
PBAs	Prussian blue analogues
Ni-PBA	$Na_2NiFe(CN)_6$
AGM	Adsorbent glass mat
NVO	Sodium Vanadate
Mn-PBA-	$Na_2MnFe(CN)_6$
MnNi-PBA-	$Na_2Mn_{0.5}Ni_{0.5}Fe(CN)_6$
CoNi-PBA	$Na_2Co_{0.5}Ni_{0.5}Fe(CN)_6$
NTP	$Na_3Ti_2(PO_4)_3$
HVO	Hydrogen Vanadate
HE-PBAs	High entropy Prussian blue analogs
HE-PBA-1	$Na_2Mn_{0.2}Fe_{0.2}Co_{0.2}Ni_{0.2}Cu_{0.2}Fe(CN)_6$
HE-PBA-2	$Na_2Mn_{0.2}Fe_{0.2}Co_{0.2}Ni_{0.2}Zn_{0.2}Fe(CN)_6$
Cu-PBA	$Na_2CuFe(CN)_6$
CB-F	Functionalized carbon black
CB-P	Pristine carbon black
PPy	Polypyrrole
LED	Light emitting diode
GCD	Galvanostatic charge discharge
PANI	Polyaniline
Co-PBA	$Na_2CoFe(CN)_6$
SWCNT	Single wall carbon nanotube
CE	Coulombic efficiency
CMC	Carboxymethyl cellulose
NaSICON	Sodium super ionic conductor
SiO_2	Silica
PBA-1	$Na_2Ni_{0.33}Co_{0.33}Mn_{0.33}Fe(CN)_6$
PBA-2	$Na_2Ni_{0.5}Co_{0.2}Mn_{0.3}Fe(CN)_6$
PBA-3	$Na_2Ni_{0.2}Co_{0.5}Mn_{0.3}Fe(CN)_6$

Chapter 1

Fundamental Aspects of Aqueous Sodium-Ion Batteries for Solar Energy Storage

Depletion of fossil fuel and global warming are the utmost concerns in modern world related to energy-environmental-crisis. The green and alternative energy sources are mandatory to save our beloved earth.[1-3] Harvesting of renewable energies from sun, wind etc. and their distribution networks should be maximized in order to accelerate the fossil fuel phase-out. The major concern of renewable energy based economy is the lack of uninterrupted supply of electricity due to the intermittent nature of energy harvesting for fluctuating weather conditions. To mitigate this issue, electrochemical energy storage systems (batteries and supercapacitors) are required to store the renewable energy efficiently and release it on demands.[4,5] In parallel, if we consider the environmental impact, we have to go for the electromobility instead of fossil fuel based vehicle economy, as transportation sectors are one of the major contributor to green-house gas emissions.[6] Therefore, electrochemical energy conversion and storage devices, *i.e.*, batteries and supercapacitors are pivotal for green and sustainable economy.[8] The batteries store energy by chemical transformations (bond breaking and formation) through diffusion-controlled Faradaic electron transfer mechanisms.[8] Energy storage mechanism for supercapacitors (specifically electrical double-layer capacitors/EDLCs) is surface-controlled nonFaradaic physical charge separation, without active electron transfer between electrode-electrolyte interfaces.[8,9] Pseudocapacitor is an another member of supercapacitor family, whereas surface-Faradaic (pseudoFaradaic) electron transfers have been taken place through the electrical double-layer. Cyclic voltammetric analysis with various scan rates provides estimations of contributory diffusion-controlled and surface-controlled processes under the following power law:[10]

$$i = a\,\upsilon^{b} \quad \text{..... (1)}$$

Whereas, i and υ are current and scan rate, respectively, and a & b are characteristic constants. The b = 0.5 suggests diffusion-controlled mechanism as per Randles-Sevcik equation, while b = 1 indicates surface-controlled mechanism.

The ratio of diffusion and surface contributions could be ascribed by the Eq. 2.[10]

$$i(\upsilon) = k_1\,\upsilon + k_2\,\upsilon^{1/2} \quad \text{..... (2)}$$

The k_1 and k_2 are the coefficients related to the surface-controlled and diffusion-controlled processes, respectively. From the kinetic perspective, Faradaic processes are sluggish than pseudo and nonFaradaic processes. By contrary, quantity of accumulated energy is much greater in Faradaic processes compare to pseudo and nonFaradaic mechanisms. Based on this argument, battery is classified as energy device, while, entire supercapacitor family is termed as power device.

In this decade, lithium ion battery is the most mature and commercially successful technology, which is widely used in consumer-electronics, electro-mobility and many other specific applications.[11] But, the cost and safety concerns are the limiting issues for this technology.[12] The applications, whereas high energy and power densities are the prerequisites, then the lithium ion technology is indispensable. Therefore, lithium ion battery is the only option in consumer electronics and electro-mobility applications. On the other hand, the prerequisites of the energy storage devices for load levelling applications are low cost, high safety, environmentally benign, long cycle life and successful operation under a wide temperature window.[13,14] In this light of the foregoing, lithium ion batteries are not suitable candidates for large scale energy storage.[15] Nevertheless, the sodium ion technology may be a good option because of its natural abundance and similar electrochemical properties to lithium ion systems.[11,16] Sodium ion batteries follow the same rocking chair principle as Li ion batteries , where Na ions move forth and back during charge and discharge, just like rocking chairs. During charge, Na ions move from the positive electrodes to negative electrodes *via* the electrolyte medium and electrons also move from the external circuit, and the reverse movements of Na ions and electrons are observed during discharge. The working principle of sodium ion batteries is depicted in Figure 1.

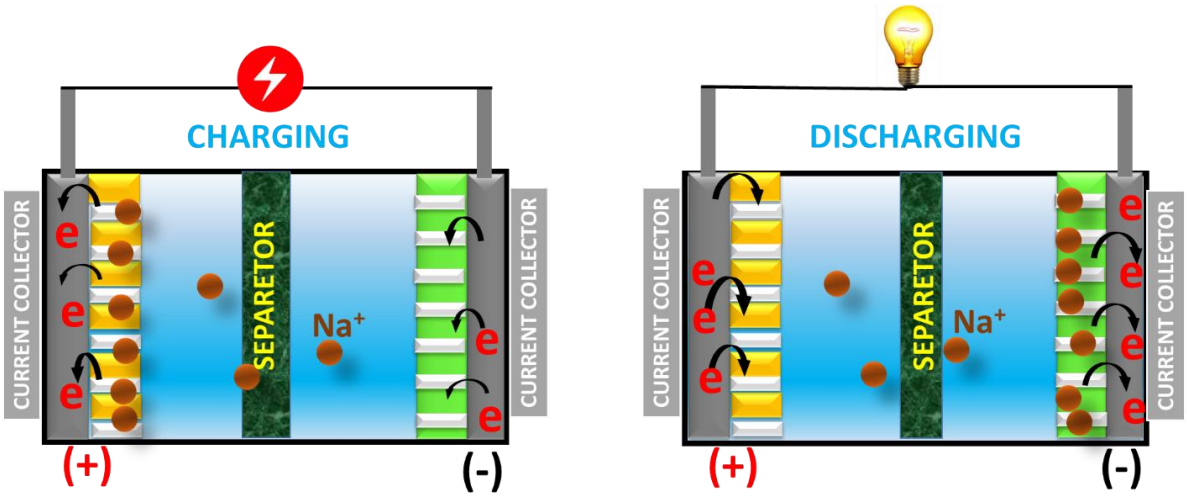

Figure 1: Working principle of Na-ion cell during charge and discharge.

Even though, both Li and Na-ion systems have similar ion intercalation/deintercalation mechanism for energy storage; but the structural features of the active materials in two systems are quite different. Because of the Shannon's ionic radii mismatch between Li^+ (0.76 Å) and Na^+ (1.02 Å) ions, the respective structures of the host lattices are differently selected in order to maintain the unrestrained solid state diffusions.[13] In this regards, the Prussian blue analogues (PBAs) with open framework structures and larger void spaces are suitable for sodium ion systems, as the size of Na^+ ion and the void spaces in the lattice structure are synchronizing.[17,18] Hence, PBAs are the important candidate for positive electrodes of sodium ion based energy storage devices. These materials could be synthesized in bulk scale under ambient conditions from the environmentally benign and low cost precursors, while

no hazardous by-products are generated.[19] Furthermore, the minimal defects and resultant lower amount of interstitial water in crystal structures are desirable for stability and electrochemical performances of PBAs, and that can be easily accomplished during the synthesis processes.[20-22] On the other hand, there are limited material resources are available for negative electrodes of aqueous sodium ion batteries. The intensified research activities are going on to screen the appropriate negative active materials, which should be characterized by high capacity, high rate capability and long life. In this regard, different classes of negative active materials, like, hard carbons, MXenes, sulphides, oxides, phosphates, etc. are widely studied for aqueous sodium ion batteries.[23]

In this thesis, diverse aqueous sodium ion batteries are developed with various configurations from positive electrode, negative electrode and electrolyte for the solar energy storage applications. Herein, the prototypes are assembled with different PBAs based positive electrodes along with multiple classes of negative electrodes in flooded and starved electrolyte configurations. In Chapter 2, $Na_2NiFe(CN)_6$ (Ni-PBA) positive electrode is coupled with functionalized carbon negative electrodes in starved electrolyte configuration, whereas adsorbent glass mat (AGM) separator is socked with 1 M Na_2SO_4 (aq.) solution. The $Na_2CoFe(CN)_6$//NaV_3O_8 (Co-PBA//NVO) batteries are assembled in both Na_2SO_4-AGM and Na_2SO_4-SiO_2-gel starved electrolyte configurations, which is demonstrated in Chapter 3. Chapter 4 demonstrates Na_2SO_4-SiO_2-gel based sodium ion batteries with $Na_2MnFe(CN)_6$ (Mn-PBA) positive and Fe_2O_3 negative electrodes. The limitations of Mn-PBA positive and Fe_2O_3 negative electrodes are mitigated by synthesizing $Na_2Mn_{0.5}Ni_{0.5}Fe(CN)_6$ (MnNi-PBA) and Na-doped Fe_2O_3 ($Na_xFe_2O_3$), respectively, while successful gel based MnNi-PBA//$Na_xFe_2O_3$ full cells are demonstrated in Chapter 5. In this chapter, a novel hybrid gel is also developed by the appropriate mixing of carboxymethyl cellulose (CMC) and SiO_2 in 1 M Na_2SO_4 that demonstrates excellent operating voltage window and durability in the assembled prototypes. Chapter 6 depicts $Na_2Co_{0.5}Ni_{0.5}Fe(CN)_6$//$Na_3Ti_2(PO_4)_3$ (CoNi-PBA//NTP) configuration in sodium ion battery, while Na_2SO_4-SiO_2 hydrogel electrolyte is employed. In chapter 7, the optimization studies of Ni/Co/Mn ratio are performed in $Ni_xCo_yMn_zFe(CN)_6$ system, and $Ni_{0.33}Co_{0.33}Mn_{0.33}Fe(CN)_6$ demonstrates optimized energy and power densities. The $Ni_{0.33}Co_{0.33}Mn_{0.33}Fe(CN)_6$ positive and hydrogen Vanadate negative electrodes are assembled in Na_2SO_4-CMC-SiO_2 hybrid hydrogel electrolyte for developing working prototype. The high entropy PBAs (HE-PBAs: $Na_2Mn_{0.2}Fe_{0.2}Co_{0.2}Ni_{0.2}Cu_{0.2}Fe(CN)_6$/HE-PBA-1 and $Na_2Mn_{0.2}Fe_{0.2}Co_{0.2}Ni_{0.2}Zn_{0.2}Fe(CN)_6$/HE-PBA-2) are introduced as positive electrodes in Chapter 8, while the HE-PBA-1 is coupled with the $Na_2CuFe(CN)_6$-derived oxide as negative electrode in Na_2SO_4-CMC-SiO_2 hybrid hydrogel electrolyte. All the seven configurations of aqueous sodium ion batteries are laboratory tested through specific capacity, Faradaic efficiency, rate capability, energy density, power density, cycle life, etc. Moreover, the prototypes are also performance tested through the solar charging modules (field trial) for the feasibility evaluations in solar energy storage applications.

References:

1. I. Dincer, *Renew. Sustain. Energy Rev.*,2000,**4**, 157–175.
2. D. Elliott, *Futures*, 2000, **32**, 261–274.
3. T. Güney, *Int. J. Sustain. Dev. World Ecol.*, 2019, **26**, 389–397.
4. W. Zhou, H. Yang and Z. Fang, *Renew. Energy*, 2008, **33**, 1413–1423.
5. D. A. G. Redpath, D. McIlveen-Wright, T. Kattakayam, N. J. Hewitt, J. Karlowski and U. Bardi, *J. Clean. Prod.*, 2011, **19**, 2034–2048.
6. S. A. Shaheen and T. E. Lipman, *IATSS Res.*, 2007, **31**, 6–20.
7. M. Winter and R. J. Brodd, *Chem. Rev.*, 2004, **104**, 4245–4269.
8. A. Burke, *J. Power Sources*, 2000, **91**, 37-50.
9. T. Brezesinski, J. Wang, J. Polleux, B. Dunn and S. H. Tolbert, *J. Am. Chem. Soc.*, 2009, **131**, 1802-1809.
10. M. Á. Muñoz-Márquez, D. Saurel, J. L. Gómez-Cámer, M. Casas-Cabanas, E. Castillo-Martínez, and T. Rojo, *Adv. Energy Mater.* 2017, **7**, 1700463.
11. M. H. Han, E. Gonzalo, G. Singh and T. Rojo, *Energy Environ. Sci.*, 2015, **8**, 81-102.
12. N. Yabuuchi, K. Kubota, M. Dahbi and S. Komaba, *Chem. Rev.*, 2014, **114**, 11636-11682.
13. K. Chayambuka, G. Mulder, D. L. Danilov and P. H. L. Notten, *Adv. Energy Mater*., 2018, **8**, 1800079.
14. Q. Liu, Z. Hu, M. Chen, C. Zou, H. Jin, S. Wang, S. L. Chou, Y. Liu and S. X. Dou, *Adv. Funct. Mater*., 2020, **30**, 1909530.
15. H. Zhang, I. Hasa and S. Passerini, *Adv. Energy Mater.*, 2018, **8**, 1870082.
16. J. Peng, W. Zhang, Q. Liu, J. Wang, S. Chou, H. Liu and S. Dou, *Adv. Mater.*, 2022, **34**, 2108384.
17. B. Xie, B. Sun, T. Gao, Y. Ma, G. Yin, P. Zuo, *Coord. Chem. Rev.*, 2022, **460**, 214478.
18. J. Qian, C. Wu, Y. Cao, Z. Ma, Y. Huang, X. Ai and H. Yang, *Adv. Energy Mater.*, 2018, **8**, 1870079.
19. X. Wu, C. Wu, C. Wei, L. Hu, J. Qian, Y. Cao, X. Ai, J. Wang and H. Yang, *ACS Appl. Mater. Interfaces.*, 2016, **8**, 5393-5399.
20. J. Song, L. Wang, Y. Lu, J. Liu, B. Guo, P. Xiao, J. J. Lee, X. Q. Yang, G. Henkelman and J. B. Goodenough, *J. Am. Chem. Soc.*, 2015, **137**, 2658-2664.
21. W. Wang, Y. Gang, Z. Hu, Z. Yan, W. Li, Y. Li, Q. F. Gu, Z. Wang, S. L. Chou, H. K. Liu and S. X. Dou, *Nat. Commun.*, 2020, **11**, 980.
22. X. Liu, Z. Liu, W. Yang, M. Wang, B. Qin, Y. Zhang, Z. Liu and H. Fan, *Mater.TodayChem.*, 2022, **26**, 101002.
23. X. Li, H. Liang, B. Qin, M. Wang, Y. Zhang and H. Fan, *J. Colloid Interface Sci.*, 2022, **625,** 41-49.

Chapter 2

Aqueous Sodium-Ion Hybrid Batteries with $Na_2NiFe(CN)_6$ Prussian Blue Analogue Positive and Functionalized Carbons Negative Electrodes in Starved Electrolyte Configuration

Introduction: Prussian blue analogues (PBAs) are a major class of redox-active compounds used as positive electrode materials for aqueous sodium ion batteries. Due to having open three-dimensional framework structures, the PBAs are capable of facile sodium ion insertion/deinsertion in/from the host lattices during charge/discharge; and deliver appreciable energy storage performances. These materials could be produced in large scale at ambient temperature through inexpensive and green routes, whereas no toxic byproducts are generated.[1] Among the several PBAs, the Ni based analogue $Na_2NiFe(CN)_6$ (Ni-PBA) is a mono-redox specie, which shows low specific capacity and delivers good cycling stability compared to other bi-redox PBAs.[2,3] For aqueous sodium ion-based systems, inexpensive, ecologically friendly carbonaceous materials with good conductivity and capacitance are frequently utilized as negative electrode materials.[4] The carbonaceous materials, like activated carbon, carbon black, etc. generally exhibit surface-controlled capacitive and pseudo-capacitive sodium ion storage mechanisms.[5]

Present work: We have synthesized a low defect Ni–PBA by using citrate assisted in *situ* co-precipitation method, and used as positive electrode material. Two distinct functionalized carbon blacks, namely (i) CB-F1 and (ii) CB-F2, are derived from pristine carbon black (CB-P), and used as the negative electrodes. Comparative performances of Ni-PBA and Ni-PBA/Polypyrrole (Ni-PBA/Ppy) composite are studied, where Ni-PBA/Ppy shows improved performances. Electrochemical measurements are carried out in 1 M Na_2SO_4 electrolyte, whereas polyaniline (PANI) coated low cost stainless steel (SS304) is used as current collector. Three different asymmetric 1.2 V full cells are assembled with (i)Ni-PBA/Ppy//CB-P, (ii) Ni-PBA/Ppy//CB-F1 and (iii) Ni-PBA/Ppy//CB-F2 configurations, whereas the 1 M Na_2SO_4 electrolyte is socked in AGM. Furthermore, for all climate operations, temperature dependence studies are performed for three asymmetric cells. Finally, a 4 V prototype device is assembled by connecting four full cells in series. The prototype device delivers a capacity of 0.21 mAh at 1 mA charge/discharge current, and retains 60 % of initial capacity over 1000 cycles within 0-4 V window. This prototype device also able illuminates 3 V/270 mW LED setup, which indicates the prospects of the device in practical applications.

Results and discussion: Electrochemical performances of positive and negative materials are tested through cyclic voltammetry (CV) and galvanostatic charge discharge (GCD) measurements. The CV analysis of positive materials is performed under 0-1.2 V *vs.* Ag/AgCl potential window at variable scan rate shown in Figure 2a. Figure 2b displays the GCD profile of Ni-PBA/Ppy at a variable C rate. Ni-PBA/Ppy delivers a specific capacity of 73.6 mAh g^{-1} and good cycle life with 70 % capacity

retention over 300 cycles at 2C rate within 0.05-1.2 V *vs.* Ag/AgCl. The CV measurement carried out for all three different carbon blacks within -0.5 to 0.5 V *vs.* Ag/AgCl at 5 mV s^{-1} scan rate (Figure 2c). The CB-F2, CB-F1 and CB-P based symmetric cells are tested and the GCD profile shown in Figure 2d, where cells deliver specific capacitances of 15, 10 and 8 F g^{-1}, respectively, at 50 mA g^{-1} current density within 0-1 V potential window. Three asymmetric cells are assembled with Ni-PBA/Ppy//CB-F2, Ni-PBA/Ppy//CB-F1, and Ni-PBA/Ppy//CB-P configurations. The comparative rate capacity profile for 3 different full cells is shown in Figure 2e, where Ni-PBA/Ppy//CB-F2 demonstrates best performance compare to others. The Ni-PBA/Ppy//CB-F2 delivers a specific capacity of 28 mAh g^{-1} with 90 % Coulombic efficiency (@ 0.2C). The Ragone plot shown in Figure 2f demonstrates comparative energy and power profile of three cells. Cycling performance also tested through GCD cycling at 1C rate within 0-1.2 V (Figure 2g). All the asymmetric cells are further tested at a wide temperature range (-10 to 50 ºC), and Ni-PBA/Ppy//CB-F2 based cell presents best results compared to others (Figure 2h). Nevertheless, the operating temperature may be considered as 0-50 ˚C for this sodium ion system. Furthermore, a 4 V prototype device is developed, which demonstrates about 60 % capacity retention over 1000 cycles at 1 mA current within 0-4 V window and is able to illuminate 3 V/270 mW LED setup. However, the aqueous sodium ion devices with Ni-PBA based positive and functionalized carbon based negative electrodes are attractive for large scale energy storage applications.

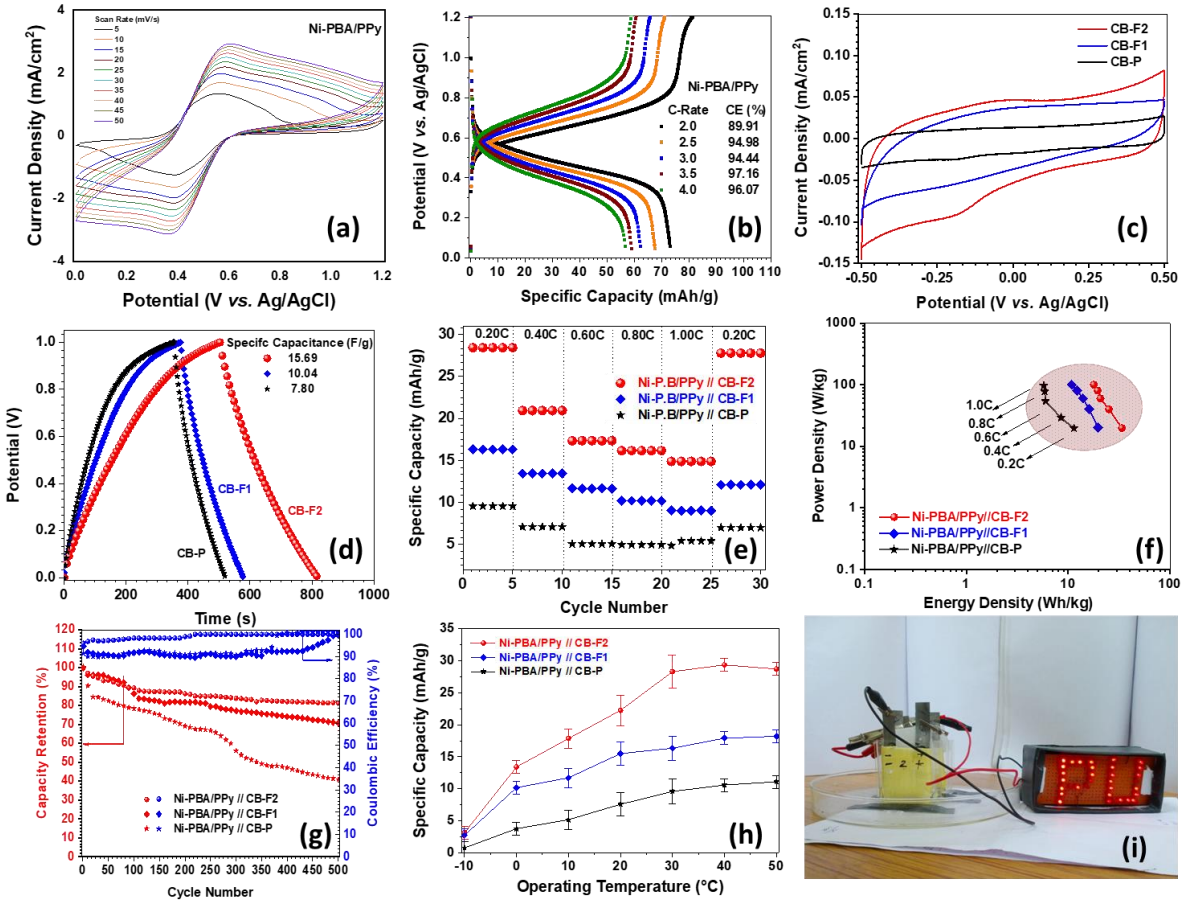

Figure 2: (a) CV profile for Ni-PBA/Ppy at 5 to 50 mV/s scan rate within 0-1.2 V *vs.* Ag/AgCl window in 1 M Na_2SO_4 medium; (b) GCD profile of Ni-PBA/Ppy at variable C rate within 0-1.2 V *vs.* Ag/AgCl regime; (c) Comparative CV profiles for CB-P, CB-F1 and CB-F2 within 0.5 to -0.5 V *vs*. Ag/AgCl window at 5 mV s^{-1} scan rate in 1 M Na_2SO_4 solution; (d) GCD profiles of symmetric full cells based on CB-P, CB-F1 and CB-F2 at 50 mA g^{-1} current density within 0-1 V potential window; (e) Rate capability studies of three asymmetric cells at various C-rates; within 0-1 V window; (f) Ragone plot: cell performances data of three asymmetric cells at various C rate; (g) GCD cycling of all three asymmetric cell at 1C rate within 0-1V; (g) specific capacity *vs*. temperature profile of all three cells; (i) photograph exhibits that 4 V device illuminates 3 V/270 mW LED setup.

Conclusions: Herein, The Ni-PBA/PPy positive electrode demonstrates improved performances compare to pristine Ni-PBA. Three asymmetric full cells are developed with Ni-PBA/PPy positive electrode and three different negative electrodes, namely CB-P, CB-F1 and CB-F2. The low-cost PANI coated SS304 current collectors are employed in this study, while PANI coating prevents the corrosion of SS under the operating voltage window. However, the aqueous sodium ion devices with Ni-PBA based positive and functionalized carbon based negative electrodes are attractive for large scale energy storage applications.

References:

1. J. Qian, C. Wu, Y. Cao, Z. Ma, Y. Huang, X. Ai and H. Yang, *Adv. Energy Mater.*, 2018, **8**, 1870079.
2. D. Yang, J. Xu, X. Z. Liao, Y. S. He, H. Liu and Z. F. Ma, *ChemComm.*, 2014, **50**, 13377-13380.
3. S. Yu, Y. Li, Y. Lu, B. Xu, Q. Wang and M. Yan, Y. Jiang, *J. Power Sources*, 2015, **275**, 45-49.
4. Y. Zhao, L. P. Wang, M. T. Sougrati, Z. Feng, Y. Leconte, A. Fisher, M. Srinivasan and Z. Xu, *Adv. Energy Mater.*, 2017, **7**, 1601424.
5. Y. Wang, L. Zhang, H. Hou, W. Xu, G. Duan, S. He, K. Liu and S. Jiang, *J. Mater. Sci.*, 2021, **56**, 173-200.

Chapter 3

Aqueous Sodium-Ion Batteries with $Na_2CoFe(CN)_6$ Prussian Blue Analogue Positive and Sodium Vanadate Negative Electrodes in Silica Gel Electrolyte

Introduction: Environmentally benign aqueous Na-ion batteries are inexpensive and have enormous potential in solar energy storage applications. Prussian blue analogues (PBAs) demonstrate promising electrochemical performances toward Na-ion systems. Due to having open framework structures it follows intercalation/deintercalation mechanism in aqueous electrolyte media.[1] Moreover, appreciable electrochemical reversibility, chemical and electrochemical stability, low-cost and non-complicated synthesis routes, good processability for large scale production and environmental friendliness promote PBAs as prospective positive materials for Na-ion batteries.[2] Layered Oxide materials are a good candidate as a negative electrode for aqueous sodium ion systems in metal oxide arena. However, limited reports are available on layered Na-vanadate compounds in the negative electrodes of Na-ion batteries.[3] The doping of Na ions into the layered V_2O_5 structure acts as a pillar that effectively improves the structural integrity of the Na-vanadate upon repetitive charge/discharge.[4]

Present work: In this work, we have synthesized $Na_2CoFe(CN)_6$ (Co-PBA) and NaV_3O_8 (NVO) as positive and negative materials, respectively. All the electrochemical performances are tested through CV and GCD analysis for both positive and negative materials. Finally, a 1.5 V Na-ion cell is developed with (+)Co-PBA//NVO(-) configuration, and studied in two different cell packing structures. Herein, a modification approach was taken to improve the performance of SS304 current collector through single wall carbon nanotube (SWCNT) coating. The SWCNT coating drastically impedes the corrosion of SS304 and enhances the water splitting window through the coverage of metal substrate from direct contact with electrolyte. The Co-PBA//NVO full cells are fabricated with appropriate mass-balancing under two different starved electrolyte configurations, namely (i) 1.2 V pouch cell with 1 M Na_2SO_4 electrolyte socked AGM separator, and (ii) 1.5 V prismatic cell with 1 M Na_2SO_4-silica gel electrolyte.

Results and discussion: Figure 3a demonstrates CV profiles of Co-PBA at variable scan rates ranging from 5 to 30 mV/s within 0-1.2 V *vs.* Ag/AgCl voltage regime. The specific capacities and associated coulombic efficiency (CE) values at different C-rates are shown in Figure 3b, while 122, 100, 90, 84 and 80 mAh g^{-1} capacities are obtained at 1, 2, 3, 4 and 5C rates, respectively. The GCD profiles of NVO at variable C-rates under 0.2 to -0.8 V are shown in Figure 3c. It delivers 83, 65, 27, 28 and 23 mAh g^{-1} specific capacities at 1, 2, 3, 4 and 5C rates. Herein, we have developed full cells configured with (+)Co-PBA//1M Na_2SO_4 (aq.)//NVO(-) under two different electrolyte systems; (i) pouch cell with electrolyte socked AGM separator, and (ii) prismatic cell with Na_2SO_4-silica gel electrolyte. Comparative rate performance profiles are shown in Figure 3e. The Ragone plot shown in Figure 3f depicts cell performances with respect to energy and power at different C rates. Figure 3g demonstrates

the comparative cycling performance data of gel based 1.5 V prismatic cell and 1.2 V pouch cell over 500 cycles at 5C rate current. The 1.5 V gel based prismatic cell delivers an energy density of 211 Wh kg^{-1} (@ 250 W kg^{-1}), a power density of 2466 W kg^{-1} (@ 94 Wh kg^{-1}) and a good durability (80 % capacity retention @ 5C) up to 500 cycles. On the other hand, the 1.2 V pouch cell demonstrates an energy density of 153 Wh kg^{-1} (@ 192 W kg^{-1}), a power density of 1912 W kg^{-1} (@ 69 Wh kg^{-1}) and excellent cycle life (90 % capacity retention @ 5C) under 500 cycles (Figure 3g). The target of this work is to demonstrate the solar energy storage applications of aqueous Na-ion batteries (Figure 3h). Herein two 1.5 V cells are series connected to develop 3 V/5 mAh rated prototype devices, which can illuminate 3 V/270 mW LED device shown in Figure 3i.

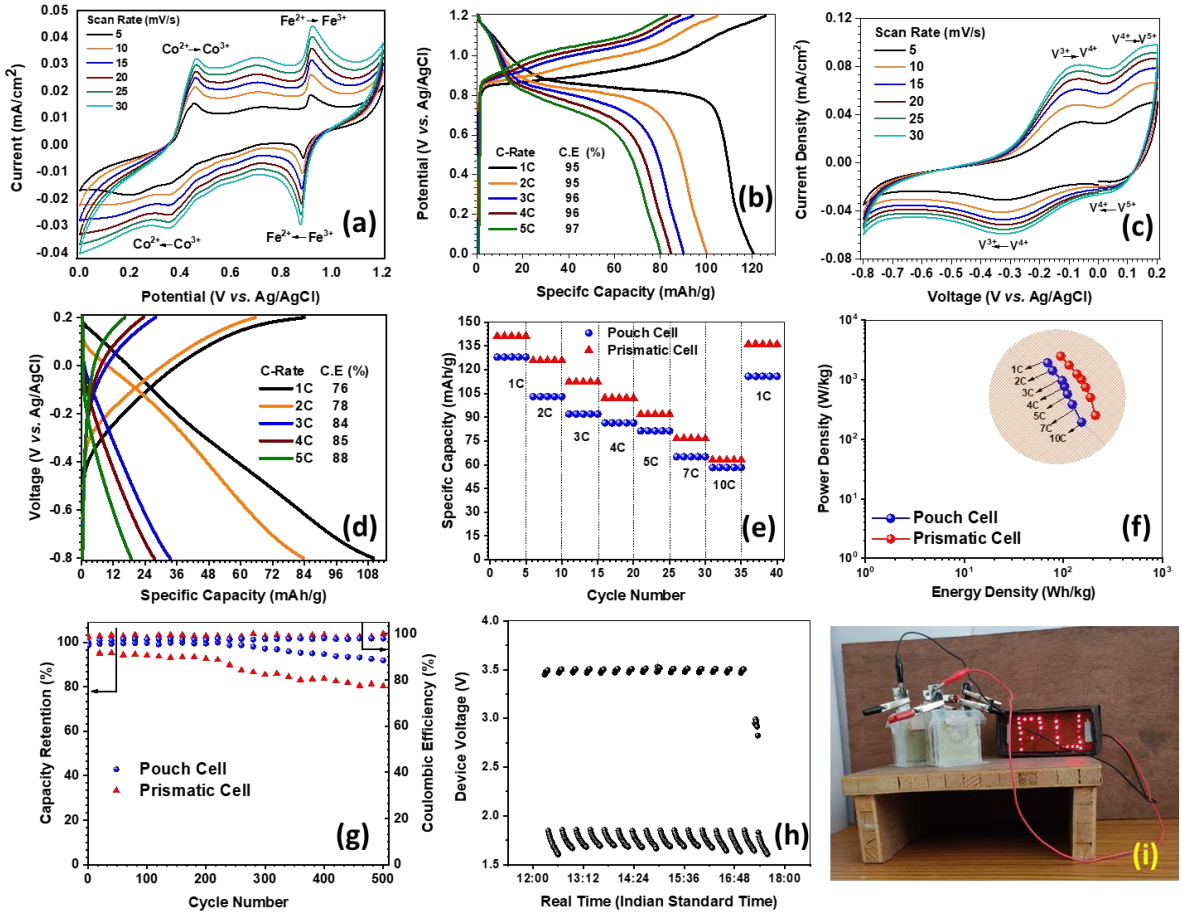

Figure 3: (a) CV Profiles of Co-PBA at scan rates of 5 to 30 mV/s within 0-1.2 V *vs.* Ag/AgCl in 1 M Na_2SO_4 medium; (b) GCD studies at different current density from 1C to 5C within 0-1.2 V *vs.* Ag/AgCl (CE values are incorporated in inset); (c) CV profiles of NVO at scan rates from 5 to 30mV/s within 0.2 to -0.8 V *vs.* Ag/AgCl in 1 M Na_2SO_4 medium; (d) GCD profile of NVO at variable C rates from 1C to 5C within 0.2 to -0.8 V *vs* .Ag/AgCl (CE values are incorporated in inset); (e) comparative rate profiles of (+)Co-PBA//NVO(-) full cells in two different configurations, namely pouch and prismatic; (f) Ragone plot: cell performance data of two different cell configurations; (g) cycling stability profiles of two different cell configurations over 500 cycles at 5C current; (h) one day voltage profile under

solar charging/LED discharging of 3 V/5 mAh device; (i) photograph exhibits a 3 V/5 mAh prototype device illuminates 3 V/270 mW LED setup.

Conclusions: Based on the performances, cost, safety, and environmental issues, as described Co-PBA//NVO device may be translated into large scale industrial productions. The high voltage operation (0-1.5 V) improves the energy storage capability and power characteristics in prismatic cell, but lowers the cycle life due to unavoidable current collector corrosion. A 3 V/5 mAh rated gel based prototype device is developed, and it demonstrates satisfactory solar energy storage performances under a week long operation.

References:

1. J. Peng, W. Zhang, Q. Liu, J. Wang, S. Chou, H. Liu and S. Dou, *Adv. Mater.*, 2022, **34**, 2108384.
2. J. Qian, C. Wu, Y. Cao, Z. Ma, Y. Huang, X. Ai and H. Yang, *Adv. Energy Mater.*, 2018, **8**, 1870079.
3. C. Deng, S. Zhang, Z. Dong and Y. Shang, *Nano Energy*, 2014, **4**, 49-55.
4. F. Wan, L. Zhang, X. Dai, X. Wang, Z. Niu and J. Chen, *Nat. Commun.*, 2018, **9**, 1656.

Chapter 4

Aqueous Sodium-Ion Hybrid Batteries with $Na_2MnFe(CN)_6$ Prussian Blue Analogue Positive and Ferric Oxide Negative Electrodes in Silica Gel Electrolyte

Introduction: Aqueous Na-ion technology is attractive for stationary applications, because of having almost all the essential characteristics which require for large scale energy storage devices.[1] The state-of-the-art aqueous Na-ion batteries demonstrate moderate energy density, but exhibit high power capability and prolonged durability, along with robust configurations.[2] Prussian blue analogues (PBAs) could be also selected for promising host materials in Na-ion systems.[3] Moreover, high theoretical capacities due to the presence of multiple active redox centers, along with low cost precursors, scalable and green synthesis methodologies make the PBAs as excellent candidates for Na-ion based energy storage devices. Among the different class of PBAs, $Na_2MnFe(CN)_6$ (Mn-PBA) is a major candidate due to presence of Mn that is nontoxic and low cost transition metal compare to Ni, and Co. Different transition metal oxides demonstrate good charge storage performances as negative electrode materials in Na-ion system. Among various metal oxides, iron oxides (FeO, Fe_2O_3, Fe_3O_4 etc.) are widely used in Na-ion based energy storage devices due to their moderate capacity, low cost and environmental friendliness.[4]

Present work: Herein, we have performed the electrochemical performance studies of low cost Mn-PBA as positive and commercial Fe_2O_3 as negative material for aqueous sodium ion batteries. CV analysis performed to evaluate the charge storage mechanism. GCD study is also carried out to evaluate the charge storage performance. All the studies are obtained by using SWCNT modified SS304 current collectors in 1 M Na_2SO_4 medium. However, full cell studies are accomplished in prismatic configuration, whereas SiO_2 based hydro-gel is used in 1 M Na_2SO_4.

Results and discussion: CV analysis of Mn-PBA is performed within the potential window of 0-1.2 V *vs.* Ag/AgCl at 20 to 40 mV/s scan rate, which is shown in Figure 4a. The GCD profiles are shown in Figure 4b, whereas Mn-PBA delivers specific capacities of 36, 32, 27, 19, and 18 mAh/g at respective current densities of 100, 200, 300, 400 and 500 mA/g. The rate performance profile is depicted in Figure 4c. The CV measurements are also carried out for commercial Fe_2O_3 to evaluate the charge storage mechanism (Figure 4d). GCD studies are performed at various current densities, while a specific capacity of 32 mAh/g is obtained at 600 mA/g current (Figure 4e). Figure 4f demonstrates rate performance of Fe_2O_3. A 1.5 V rated full cell is assembled with Mn-PBA//Fe_2O_3 configuration by using SiO_2-based gel in 1 M Na_2SO_4. The GCD and rate profiles of full cell are shown in Figure 4g & h, while the cycling performance is carried out at 300 mA/g current. Figure 4i demonstrates the durability study, whereas the capacity retention is obtained only 41% over 500 cycles.

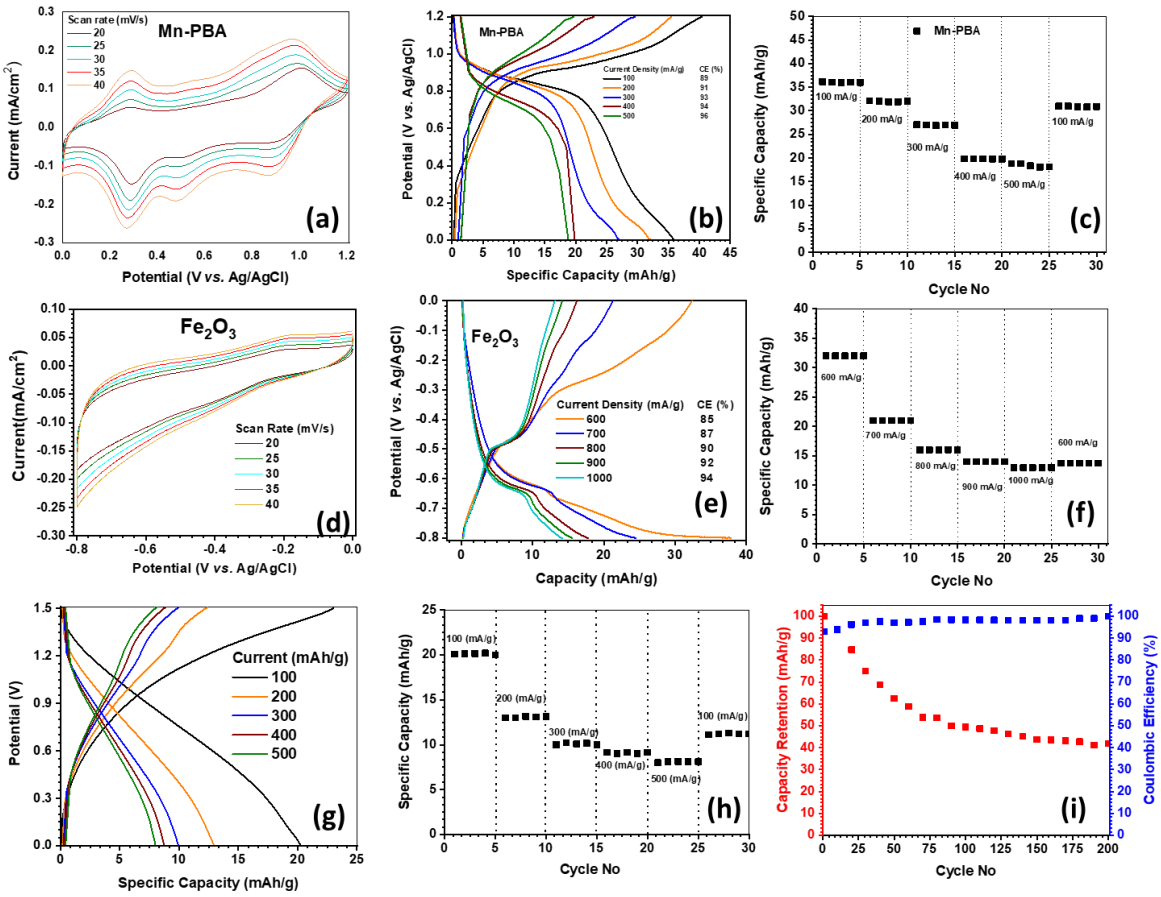

Figure 4: (a) CV profiles of Mn-PBA at 20 to 40 mV/s scan rate within 0-1.2 V *vs.* Ag/AgCl in 1 M Na_2SO_4 medium; (b) GCD profiles of Mn-PBA under 0-1.2 V *vs.* Ag/AgCl window at 100 to 500 mA/g current density; (c) rate capability profile of Mn-PBA over 30 cycles (d) CV profiles of Fe_2O_3 at scan rate of 20-40 mV/s within 0 to -0.8 V *vs.* Ag/AgCl in 1 M Na_2SO_4 medium ; (e) GCD profiles of Fe_2O_3 at 600 to 1000 mA/g current within 0 to -0.8 V *vs.* Ag/AgCl window; (f) rate capability data profile of Fe_2O_3 over 30 cycles; (g) GCD profile of Mn-PBA//Fe_2O_3 full cell by using CMC-SiO_2 based gel in 1 M Na_2SO_4 electrolyte within 0-1.5 V at 100 to 500 mA/g current ; (h) rate capability profile of 1.5 V Mn-PBA//Fe_2O_3 full cell; (i) durability data over 200 cycles at 300 mA/g current.

Conclusions: Though Mn-PBA and Fe_2O_3 are low cost and environmentally benign, but their charge storage performances are not up to the mark for developing aqueous sodium ion devices for solar energy storage applications. The mitigation strategies are developed in the next chapter.

References:

1. Z. Y. Gu, Y. L. Heng, J. Z. Guo, J. M. Cao, X. T. Wang, X. X. Zhao, Z. H. Sun, S. H. Zheng, H. J. Liang, B. Li and X. L. Wu, *Nano Res.*, 2023, **16**, 439–448.
2. Z. Y. Gu, J. Z. Guo, Z. H. Sun, X. X. Zhao, X. T. Wang, H. J. Liang, X. L. Wu and Y. Liu, *Cell Reports Physical Science*, 2021, **2**, 100665.

3. J. Peng, Zhang, Q. Liu, J. Wang, S. Chou, H. Liu and S. Dou, *Adv. Mater.*, 2022, **34**, 2108384.
4. T. Li, A. Qin, L. Yang, J. Chen, Q. Wang, D. Zhang and H. Yang, *ACS Appl. Mater. Interfaces*, 2017, **9** , 19900-19907.

Chapter 5

Aqueous Sodium-Ion Hybrid Batteries with $Na_2Mn_{0.5}Ni_{0.5}Fe(CN)_6$ Prussian Blue Analogue Positive and Na-Doped Ferric Oxide Negative Electrodes in Carboxymethyl Cellulose-Silica Gel Electrolyte

Introduction: $Na_2MnFe(CN)_6$ (Mn-PBA) positive and commercial Fe_2O_3 negative electrode materials do not match the criteria of aqueous sodium ion batteries for stationary applications, because of the poor cyclic stability.[1] The poor cycle life of positive active material is expected due to the lower intrinsic electronic conductivity and the Mn-dissolution, while the latter is caused by the Jahn-Teller distortion and disproportionation of Mn^{3+} species.[2] On the other hand, mono-redox $Na_2NiFe(CN)_6$ (Ni-PBA),whereas Ni^{2+}-centre is electrochemically inactive, delivers lower specific capacity, but the cycling stability is much better than that of Mn-PBA.[3] The Ni^{2+}-centre (d^8 electronic system) is free from the Jahn-Teller distortion, and the same is responsible for structural integrity upon repetitive charge/discharge cycles.[4] However, the Mn-Ni-based PBA, namely $Na_2Mn_{0.5}Ni_{0.5}Fe(CN)_6$ (MnNi-PBA) delivers optimized performances in both capacity and durability. In order to optimize the capacity and stability of the negative active material, the $Na_xFe_2O_3$ is synthesized from the commercial Fe_2O_3. A 1.5 V cell is assembled with MnNi-PBA positive and $Na_xFe_2O_3$ negative electrodes in Na_2SO_4-CMC-SiO_2 hybrid gel electrolyte, whereas, the prototype device delivers decent performances for solar storage applications.

Present work: In this work, we have thoroughly studied the structural, morphological and electrochemical characteristics of low cost MnNi-PBA positive electrodes and $Na_xFe_2O_3$ negative electrodes for aqueous Na-ion batteries. We have found that the MnNi-PBA demonstrates promising charge storage capacity and $Na_xFe_2O_3$ shows decent electrode performance compare to Mn-PBA and $Na_xFe_2O_3$, respectively. Moreover, the charge storage mechanisms of MnNi-PBA positive and $Na_xFe_2O_3$ negative electrodes are elucidated from variable scan rate CV analysis. Based on the electrochemical performances of positive and negative active materials, a 1.5 V full cell is assembled with (+)$Na_2Mn_{0.5}Ni_{0.5}Fe(CN)_6$//1 M Na_2SO_4//$Na_xFe_2O_3$(-) configuration in low cost CMC-SiO_2 hydrogel electrolyte, and the prototype device depicts excellent solar storage performances.

Results and discussion: The CV profiles of MnNi-PBA are shown in Figure 5a, which demonstrate diffusion controlled charge storage mechanism. The Figure 5b depicts the GCD profiles of MnNi-PBA, and this material shows specific capacities of 47 (CE = 98 %), 38 (CE = 99 %), 34 (CE = 99 %), 31 (CE = 99 %) and 28 (CE = 99 %) mAh g^{-1} under respective 100, 200, 300, 400 and 500 mA g^{-1} current densities. The $Na_xFe_2O_3$ demonstrates quasi-rectangular CV profiles (Figure 5c) with broad humps in anodic and cathodic branches within the potential window of 0 to -0.8 V *vs*. Ag/AgCl. Figure 5d demonstrate the GCD profiles of $Na_xFe_2O_3$ with CE values under various current densities, ranging from

600 to 1000 mA g^{-1}. The $Na_xFe_2O_3$ shows respective specific capacities of 53 (CE = 87 %), 51 (CE = 91 %), 48 (CE = 92 %), 46 (CE = 93 %), and 40 (CE = 96 %) mAh g^{-1}. Figure 5e demonstrates the GCD profiles of the full cell under 50-250 mA g^{-1} current densities. The full cell delivers a specific capacity of 48 mAh g^{-1} (@ 50 mA g^{-1}), an energy density of 77 Wh kg^{-1} (@ 118 W kg^{-1}), a power density of 803 W kg^{-1} (@ 56 Wh kg^{-1}), which is shown in the Ragone plot (Figure 5f). The cell deliveres a promising cycle life (80 % capacity retention after 250 cycles at 50 mA g^{-1}) under 0-1.6 V voltage window (Figure 5g). Finally, a 3.2 V prototype device is fabricated by a series combination of two 1.6 V cells in order to demonstrate the solar energy storage applications. The Figure 5h depicts the voltage profile of the prototype device under solar charge/LED load discharge schedule for one full day trial. Further, the 3.2 V device is capable to illuminate a 3 V/270 mW LED setup, which is captured in the Figure 5i.

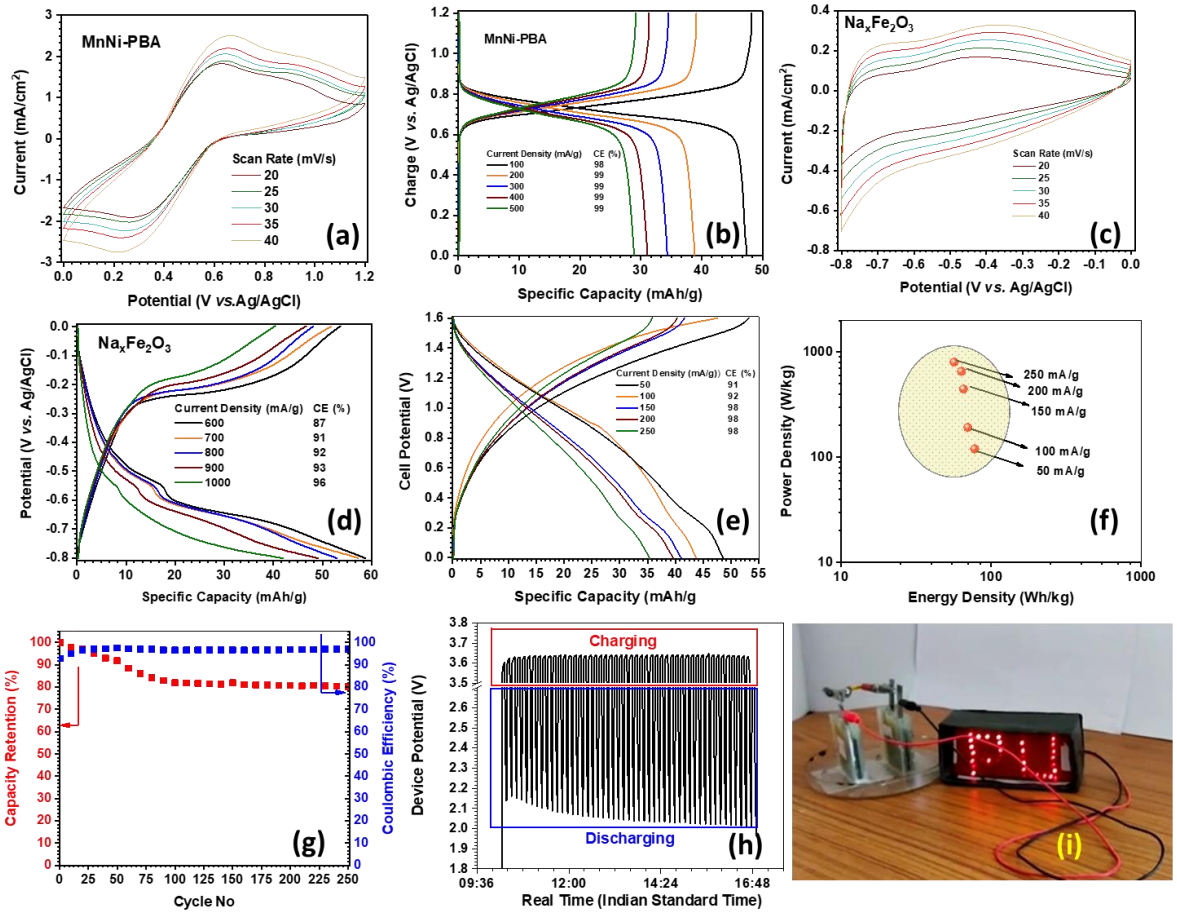

Figure 5: (a) CV profiles of MnNi-PBA at scan rates of 20-40 mV/s within 0-1.2 V *vs.* Ag/AgCl; (b) GCD profiles of MnNi-PBA within 0-1.2 V *vs.* Ag/AgCl potential at current density of 100-500 mA/g; (c) CV profiles of $Na_xFe_2O_3$ under 0 to -0.8 V *vs.* Ag/AgCl window at scan rate of 20 to 40 mV/s; (d) GCD profiles of $Na_xFe_2O_3$ within 0 to -0.8 V *vs.* Ag/AgCl regime at 600 to 1000 mA/g current; (e) GCD profiles of MnNi- PBA//1 M Na_2SO_4//$Na_xFe_2O_3$ full cell at 50 to 250 mA/g current densities in CMC-SiO_2 hybrid gel medium; (f) Ragon plot: demonstrate energy and power capability of full cell; (g)

cycling performance of 1.6 V MnNi-PBA//$Na_xFe_2O_3$ full cell over 250 cycle at 50 mA/g current; (h) voltage profile of 3 V prototype device under solar charge/LED load discharge schedule; (i) photograph exhibits that 3 V rated device illuminates 3 V/270 mW LED setup

Conclusions: The Ni-incorporation in MnNi-PBA enhances the overall charge storage performances of MnNi-PBA than that of Mn-PBA. Similarly, Na incorporated $Na_XFe_2O_3$ delivers better charge storage capabilities and durability than commercial Fe_2O_3. A MnNi-PBA//1 M Na_2SO_4//$Na_xFe_2O_3$ full cell is assembled and tested, while it depicts appreciable battery performances for large scale solar energy storage applications.

References:

1. H. Yi, R. Qin, S. Ding, Y. Wang, S. Li, Q. Zhao and F. Pan, *Adv. Funct. Mater.*, 2021, **31**, 2006970.
2. A. Banerjee, Y. Shilina, B. Ziv, J. M. Ziegelbauer, S. Luski, D. Aurbach and I. C. Halalay, *J. Am. Chem. Soc.* 2017, **139**, 1738-1741.
3. S. Yu, Y. Li, Y. Lu, B. Xu, Q. Wang, M. Yan and Y. Jiang, *J. Power Sources*, 2015, **275**, 45-49.
4. F. Gebert, D. L. Cortie, J. C. Bouwer, W. Wang, Z. Yan, S. X. Dou and S. L. Chou, *Angew. Chem. Int. Ed.*, 2021, **60**, 18519-18526.

Chapter 6

Aqueous Sodium-Ion Batteries with $Na_2Co_{0.5}Ni_{0.5}Fe(CN)_6$ Prussian Blue Analogue Positive and Sodium Titanium Phosphate Negative Electrodes in Silica Gel Electrolyte

Introduction: Aqueous Na-ion batteries are promising for solar energy storage applications. Prussian blue analogues (PBAs) are an important class of positive electrode material in Na-ion based aqueous energy storage devices, due to having (i) multiple redox centers, (ii) open framework structure, (iii) tunable compositions and structures, (iv) low cost precursors, (v) green synthesis and (vi) easy scale-up.[1-3] On the other hand, sodium superionic conductor (NaSICON) type structure is competent for negative materials, whereas Na-ion intercalation/deintercalation kinetics are very much facile.[4] The general chemical formula of NaSICON is $A_xM_yM'_{2-y}(XO_4)_3$, whereas A is an alkali or alkaline earth metal; M and M′ are transition metals and X is non-metals.[5] Several NaSICON structured materials are reported in Na-ion batteries.

Present work: From our previous studies, it is evident that the Ni-PBA shows excellent cycling life, whereas Co-PBA shows high capacity. In this work, an aqueous Na-ion battery is developed for solar energy storage applications, whereas $Na_2Co_{0.5}Ni_{0.5}Fe(CN)_6$ (CoNi-PBA) positive and NaSICON structured $NaTi_2(PO_4)_3$ (NTP) negative electrodes are employed in Na_2SO_4-SiO_2 gel electrolyte. Herein, we have opted Ni^{2+} included tri-transition metallic (bi-redox) PBA as positive electrode, and graphitic additive is used in NTP negative electrode for better durability. Resultantly, the CoNi-PBA//NTP full cell demonstrates brilliant cycle life, *i.e.*, 93 % capacity retention with 99 % Columbic efficiency (CE) over 1000 cycles at 200 mA g^{-1}. Along with that, the cell exhibits a specific capacity of 48 mAh g^{-1} (@ 100 mA g^{-1}), an energy density of 95.68 Wh kg^{-1} (@ 259.96 W kg^{-1}) and a power density of 779.75 W kg^{-1} (@ 54.36 Wh kg^{-1}). Finally, a 5 V/5 mAh prototype device is fabricated that depicts successful field trial through solar-charging cum constant-load-discharging over the period of one month.

Results and discussion: A 1.8 V cell is constructed with open framework structured CoNi-PBA positive and NTP negative electrodes in 1 M Na_2SO_4-SiO_2 hydrogel electrolyte. Both positive and negative active materials demonstrate Faradaic charge storage mechanism with appreciable diffusion coefficients, such as 5.17×10^{-15} and 1.13×10^{-15} cm^2 s^{-1}, respectively. Figure 6a represents the CV profile of CoNi-PBA at 5 to 50 mV/s scan rate within 0-1.2 V *vs.* Ag/AgCl. The GCD profile is shown in Figure 6b at a current density of 100 to 500 mA/g with coulombic efficiency inset. The CV profile of NTP is depicted in Figure 6c within the range of 0 to -0.8 V *vs.* Ag/AgCl at a scan rate of 5 to 50 mV/s, and the GCD profile is also shown in Figure 6d under the same potential window at a current density of 100 to 500 mA/g with coulombic efficiency shown in inset. The GCD profile of 1.8 V full cell configured with CoNi-PBA//1 M Na_2SO_4-SiO_2//NTP is demonstrated in Figure 6e. The Ragone plot shown in Figure 6f displays the comparative energy and power at different current densities. The

1.8 V full cell depicts a specific capacity of 48 mAh g^{-1} (@ 100 mA g^{-1}), an energy density of 95.68 Wh kg^{-1} (@ 259.96 W kg^{-1}) and a power density of 779.75 W kg^{-1} (@ 54.36 Wh kg^{-1}). The cell also exhibits excellent durability, *i.e.*, 93 % capacity retention with 99 % Columbic efficiency at 200 mA g^{-1} upon 1000 cycles (Figure 6g). A successful solar energy storage is accomplished in a 5 V/5 mAh rated Na-ion battery, which is customized by a series connection of three 1.8 V unit cells. However, the 5 V battery is performance tested under solar-charging cum constant-load-discharging experiment for one-month, and the device describes 85 % capacity retention over the period. A one-day solar performance data is displayed in Figure 6h. Figure 6i depicts the illumination of 5 V/250 mW LED by 5 V/5 mAh prototype device.

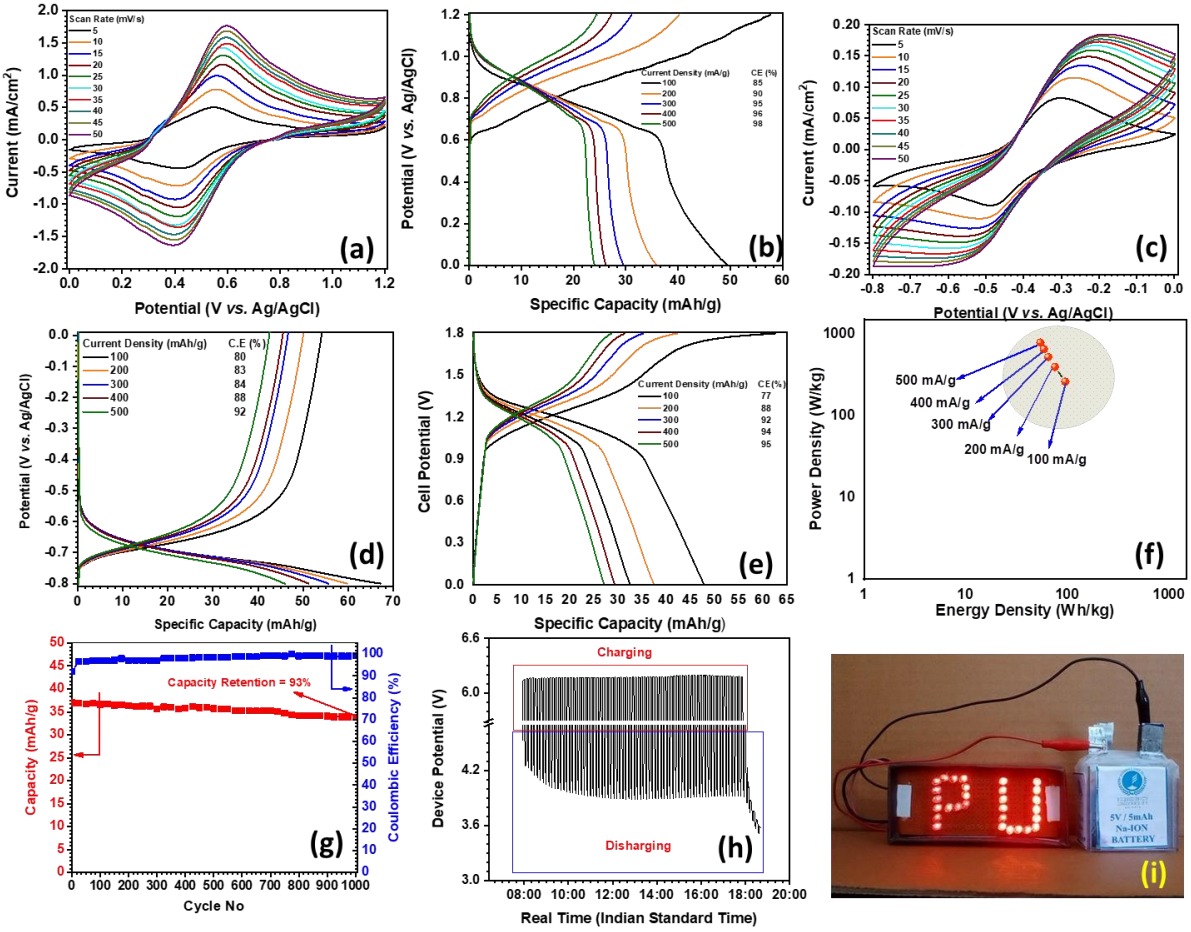

Figure 6: (a) CV profiles of CoNi-PBA at variable scan rate from 5 to 50 mV/s within 0-1.2 V *vs.* Ag/AgCl window in 1 M Na_2SO_4 medium; (b) GCD profiles of CoNi-PBA within 0-1.2 V *vs.* Ag/AgCl at 100 to 500 mA/g currents; (c) CV profiles of NTP at 5 to 50 mV/s scan rate within 0 to -0.8 V *vs.* Ag/AgCl window in 1 M Na_2SO_4 medium; (d) GCD profiles of NTP at current densities of 100 to 500 mA/g within 0 to -0.8 V *vs.* Ag/AgCl. (e) GCD profiles of CoNi-PBA//NTP full cell in 1 M Na_2SO_4-SiO2 based gel electrolyte within 0-1.8 V window at 100 to 500 mA/g current densities; (f) Ragone plot; showing the energy and power density of CoNi-PBA//NTP full cell; (g) Durability of 1.8 V full

cell at 300 mA/g current over 500 cycles; (h) one day voltage profile of 5 V/5 mAh device under solar charge/constant load discharge experiment; (i) 5 V device illuminates a 5V/250 mW LED .

Conclusions: The CoNi-PBA//NTP full cell demonstrates appreciable capacity and durability towards solar energy storage applications. Besides the substantial charge storage performances, the CoNi-PBA//NTP device is developed with low cost and environmentally benign materials and processes. Hence, the scale-up of this system is feasible, which promotes industrial validation cum commercial accomplishment.

Reference:

1. K. Hurlbutt, S. Wheeler, I. Capone and M. Pasta, *Joule*, 2018, **2**, 1950-1960.
2. G. Du and H. Pang, *Energy Storage Mater.*, 2021, **36**, 387-408.
3. Q. Wang, J. Li, H. Jin, S. Xin and H. Gao, *InfoMat*., 2022, **4**, e12311.
4. S. Chen, C. Wu, L. Shen, C. Zhu, Y. Huang, K. Xi, J. Maier and Y. Yu, *Adv. Mater.*, 2017, **29,** 1700431.
5. P. Naskar, D. Kundu, A. Maiti, P. Chakraborty, B. Biswas and A. Banerjee, *ChemElectroChem*, 2021, **8**, 1393-1429.

Chapter 7

Aqueous Sodium-Ion Batteries with $Na_2Ni_{0.33}Co_{0.33}Mn_{0.33}Fe(CN)_6$ Prussian Blue Analogue Positive and Hydrogen Vanadate Negative Electrodes in Carboxymethyl Cellulose-Silica Gel Electrolyte

Introduction:

Sodium ion batteries are the most promising alternative energy storage systems for large scale solar energy storage applications. Low cost and large scale storage systems require inexpensive and readily available materials. In this regard, sodium ion batteries meet all requirements.[1] Amid the diverse classes of active materials, Prussian blue and its analogues (PB & PBAs) are promising for positive electrodes in Na-ion systems, due to having (i) multiple redox centers, (ii) open framework structure, (iii) tunable compositions and structures, (iv) low cost precursors, (v) green synthesis and (vi) easy scale-up. PBAs are the family of coordination polymers with the generic structure of $A_xM_y[M'(CN)_6]\cdot nH_2O$, whereas A is alkali metals (Li, Na, K), M and M' are transition metals coordinated with CN ligand through respective Nitrogen- and Carbon-ends.[2] In the metallic oxide segment, vanadium based polyoxometalates (POMs) are promising candidates for the negative electrode of aqueous Na-ion batteries due to the following reasons: (i) high storage capacity because of multielectronic redox activity, and (ii) high power capability due to facile Na-ion diffusion through the open layered structure.[3] Hydrogen Vanadate (HVO) is a potential candidate for an aqueous sodium ion battery negative electrode.[4]

Present work:

In this work, we have synthesized three different tetra-transition metallic PBAs, namely (i) $Na_2Ni_{0.33}Co_{0.33}Mn_{0.33}Fe(CN)_6$ (PBA-1), (ii) $Na_2Ni_{0.5}Co_{0.2}Mn_{0.3}Fe(CN)_6$ (PBA-2) and (iii) $Na_2Ni_{0.2}Co_{0.5}Mn_{0.3}Fe(CN)_6$ (PBA-3) as positive electrode materials and hydrogen vanadate (HVO) as negative electrode material for hydrogel based Na-ion batteries. The synthesized positive and negative active materials are thoroughly characterized by various physicochemical and electrochemical methods. Based on the comparative electrochemical performances of PBA-1, PBA-2 and PBA-3, PBA-1 is selected as a positive active material in Na-ion full cell. Therefore, a 1.8 V PBA-1//HVO full cell is assembled in 1 M Na_2SO_4-carboxymethylcellulose (CMC)-silica (SiO_2) based hydrogel electrolyte. The full cell demonstrates a specific capacity of 65 mAh g^{-1} (@100 mA g^{-1}), an energy density of 118 Wh kg^{-1} (@ 181 W kg^{-1}), a power density of 780 W kg^{-1} (@ 46 Wh kg^{-1}) and a good cycle life (81% capacity retention upon 500 cycles @ 300 mA g^{-1}). A 5 V/4 mAh prototype device is developed for the practical demonstration of solar energy storage applications.

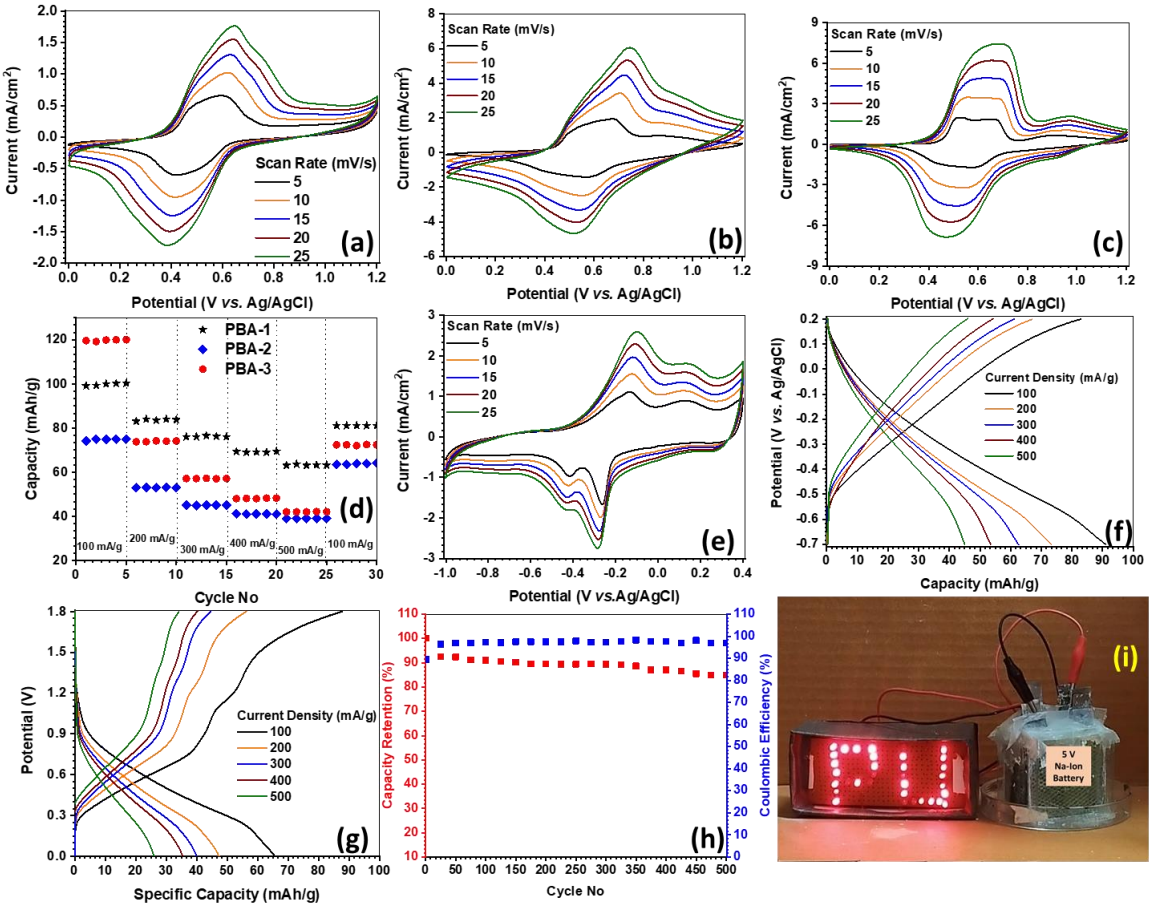

Figure 7: CV profile of PBAs within 0-1.2 V *vs.* Ag/AgCl at scan rate of 0-25 mV/s shown in (a) PBA-1, (b) PBA-2 and (c) PBA-3; (d) rate capability profile of PBAs 100 to 500 mA/g current density; (e) CV profile of HVO within 0.4 to -1.0 V *vs.* Ag/AgCl at 5-25 mV/s scan rate; (f) GCD profile of HVO at 100-500 mA/g current density within 0.2 to -0.7 V *vs.* Ag/AgCl; (g) GCD profile of PBA-1//HVO full cell within 0-1.8 V at 100-500 mA/g current; (h) cycle life data over 500 cycles at 300 mA/g; (i) 5V prototype device illuminating 3V/270 mW LED.

Result and discussion:

CV profiles of PBAs are shown in Figures 7a-c within 0-1.2 V *vs.* Ag/AgCl, whereas prominent anodic/cathodic redox pairs are noted at 0.60/0.40, 0.67/0.56 and 0.61/0.42 V in PBA-1, PBA-2, and PBA-3, respectively. The redox activities arise in PBAs from the $Co^{2+/3+}$, $Mn^{2+/3+}$ and $Fe^{2+/3+}$ redox pairs; while Ni^{2+} is electrochemically inert and not contributes to the charge storage capacity of the materials. The rate capability data is presented in Figure 7d, whereas 32, 47 and 65 % capacity degradations are observed for PBA-1, PBA-2 and PBA-3, respectively, when current density increases from 100 to 500 mA g^{-1}. The rate capability data are also interpreted by the capacity retention values after 25 cycles by returning the current at 100 mA g^{-1}; whereas PBA-1 (81 %) and PBA-2 (84 %) depict better retention

compared to PBA-3 (60 %). The CV measurements of HVO are carried out within 0.4 to -1.0 V *vs.* Ag/AgCl potential window at 5-25 mV s^{-1}, while the voltammograms are shown in Figure 7e. There are two distinct cathodic/anodic redox peak pairs found at around -0.26/0.86 and -0.41/-0.12 V, which correspond to respective $V^{5+}/^{4+}$ and $V^{4+}/^{3+}$ redox couples. The GCD profiles of HVO at variable current loads (100-500 mA g^{-1}) within 0.2 to -0.7 V range are shown in Figure 7f. The HVO exhibits respective specific capacities of 82 (CE = 91 %), 67 (CE = 91 %), 61 (CE = 99 %), 54 (CE = 98 %) and 46 (CE = 99 %) mAh g^{-1} at 100, 200, 300, 400 and 500 mA g^{-1} current density. A PBA-1//HVO full cell is assembled with a positive limited configuration in CMC-SiO_2-Na_2SO_4 hydrogel electrolyte. Figure 7g demonstrates the GCD profiles of full cell, while 65 (CE = 75 %), 47 (CE = 85 %), 40 (CE = 89 %), 35 (CE = 89 %), and 26 (CE = 92 %) mAh g^{-1} specific capacities are manifested under respective 100, 200, 300, 400 and 500 mA g^{-1} current densities within 0-1.8 V. Figure 7h demonstrates the cycle life data of the full cell, which shows 81 % capacity retention with 91 % CE upon 500 cycles at 300 mA g^{-1} current density. To demonstrate the solar energy storage performances, a 5 V/4 mAh rated prototype device is developed by series connection of three 1.8 V cells, while each 1.8 cell is fabricated by using two positive and two negative electrodes in parallel connections. 5 V prototype device illuminates a 3V/270 mW LED light set up, which is presented in Figure 7i.

Conclusion:

The PBA-3 shows highest capacity (120 mAh g^{-1}) than that of PBA-1 (100 mAh g^{-1}) and PBA-2 (75 mAh g^{-1}) at 100 mA g^{-1} current load, while it demonstrates poor rate capability (65 % capacity loss from 100-500 mA g^{-1}) and durability (86 % capacity retention upon 500 cycles @ 300 mA g^{-1}). Besides, PBA-1 and PBA-2 depict better performances on rate capability (32 and 47 %, respectively) and durability (91 and 92 %, respectively). However, this performance matrix identifies PBA-1 as the optimally suitable candidate for the positive electrode of aqueous Na-ion full cell. Herein, we have synthesized HVO as a negative active material, and the same is thoroughly characterized by physicochemical and electrochemical means. We have assembled a 1.8 V PBA-1//HVO full cell in hydrogel electrolyte, and this cell exhibits good performance. Finally, we have validated the integration of a 5 V/ 4 mAh prototype device for practical demonstration of solar energy storage applications.

References:

1. Z. Y. Gu, Y. L. Heng, J. Z. Guo, J. M. Cao, X. T. Wang, X. X. Zhao, Z. H. Sun, S. H. Zheng, H. J. Liang, B. Li and X. L. Wu, *Nano Res.*, 2023, **16**, 439–448.
2. L. L. Zhang, C. Wei, X. Y. Fu, Z.Y. Chen, B. Yan, P. P Sun, K. J. Chang and X. L. Yang, *Carbon Energy*, 2021, **3**, 827-839.
3. X. Zhang, Z. Zhang, S. Xu, C. Xu and X. Rui, *Adv. Funct. Mater.*, 2023, ***33***, 2306055.
4. D. Wang, Q. Wei, J. Sheng, P. Hu, M. Yan, R. Sun, X. Xu, Q. An and L. Mai, *Phys.Chem. Chem.Phys.*, 2016, **18**, 12074-12079.

Chapter 8

Aqueous Sodium-Ion Batteries with High-Entropy $Na_2Mn_{0.2}Fe_{0.2}Co_{0.2}Ni_{0.2}Cu_{0.2}Fe(CN)_6$ Prussian Blue Analogue Positive and $Na_2CuFe(CN)_6$-Derived Oxide Negative Electrodes in Carboxymethyl Cellulose-Silica Gel Electrolyte

Introduction:

Gradually phasing out of fossil fuel based economy, and concomitant phasing into sustainable energy based economy needs economically feasible large scale energy storage systems, due to the intermittent nature of renewable energy sources. Battery technologies are an appropriate candidate for large scale energy storage systems. Na ion batteries are the most attractive candidates for low cost, natural abundance, and environmental friendliness. High entropy Prussian blue analogs (HE-PBAs) are being tested for positive electrodes in Na-ion batteries due to their; (i) redox activity, (ii) open framework structures and (iii) easy scale up.[1,2] Metal oxides are also studied for negative materials in aqueous sodium ion batteries.[3] Among different classes of oxide materials, Prussian blue derived oxides could be a promising candidate as negative active material.[4]

Present Work

In this study, we have synthesized two different HE-PBAs, namely $Na_2Mn_{0.2}Fe_{0.2}Co_{0.2}Ni_{0.2}Cu_{0.2}Fe(CN)_6$ (HE-PBA-1) and $Na_2Mn_{0.2}Fe_{0.2}Co_{0.2}Ni_{0.2}Zn_{0.2}Fe(CN)_6$ (HE-PBA-2) for positive electrode, while these are physicochemically and electrochemically characterized. The $Na_2CuFe(CN)_6$ (Cu-PBA) derived oxides (PBA-derived oxide) are also synthesized for negative active materials. The synthesized materials are tested through cyclic voltammetry (CV) and galvanostatic charge-discharge (GCD) measurements. A 2 V full cell is assembled, and configured with HE-PBA-1//PBA-derived oxide in CMC-SiO_2-1 M Na_2SO_4 electrolyte. A 4 V device is developed by a series connection of two 2 V individual cells. The 4 V device is capable of taking solar charge and can illuminate 3V/270 mW rated LED device.

Result and Discussion

Cyclic voltammetry measurements are carried out for positive materials, namely HE-PBA-1 and HE-PBA-2, within 0-1.2 V *vs.* Ag/AgCl at a scan rate of 5 to 25 mV/s (Figure 8a,b). HE-PBA-1 delivers specific capacities of 70, 62, 58, 54, and 52 mAh/g at 100, 200, 300, 400 and 500 mA/g, respectively. Whereas HE-PBA-2 delivers respective 66, 56, 47, 44 and 41 mAh/g at similar current densities. Comparative rate capability profiles are shown in Figure 8c. HE-PBA-1 retains a capacity of 75% from 100 to 500 mA/g, however 66% capacity retention is only observed for HE-PBA-2. These results demonstrate HE-PBA-1 delivers comparatively better performance as positive material than HE-PBA-2. The CV measurements are carried out for PBA-derived oxide shown in Figure 8d. The GCD profile

is shown in Figure 8e where it delivers a specific capacity of 51, 42, 33, 28, and 23 mAh/g at current densities of 100, 200, 300, 400 & 500 mA/g, respectively, within 0 to -0.7 V *vs.* Ag/AgCl. Over 25 cycles it retains a specific capacity of 92 %. Figure 8f represents the GCD profile of the 2 V full cell, where it delivers a specific capacity of 64, 54, 46, 40 & 36 mAh/g at 100 to 500 mA/g current, respectively. The cell achieves an energy density of 128 Wh/kg (@199 W/kg) and a power density of 993 W/kg (@ 72 Wh/kg). The Ragone plot is depicted in Figure 8g. The stability performance of the cell is measured through GCD cycling at 200 mA/g current density, and 81 % capacity retention, with 100 % coulombic efficiency observed over 500 cycles (Figure 8h). A 4 V device is assembled by configuring two 2 V cells in a series connection, which is capable of accepting solar charging and illuminating 3V/270 mW LED setup.

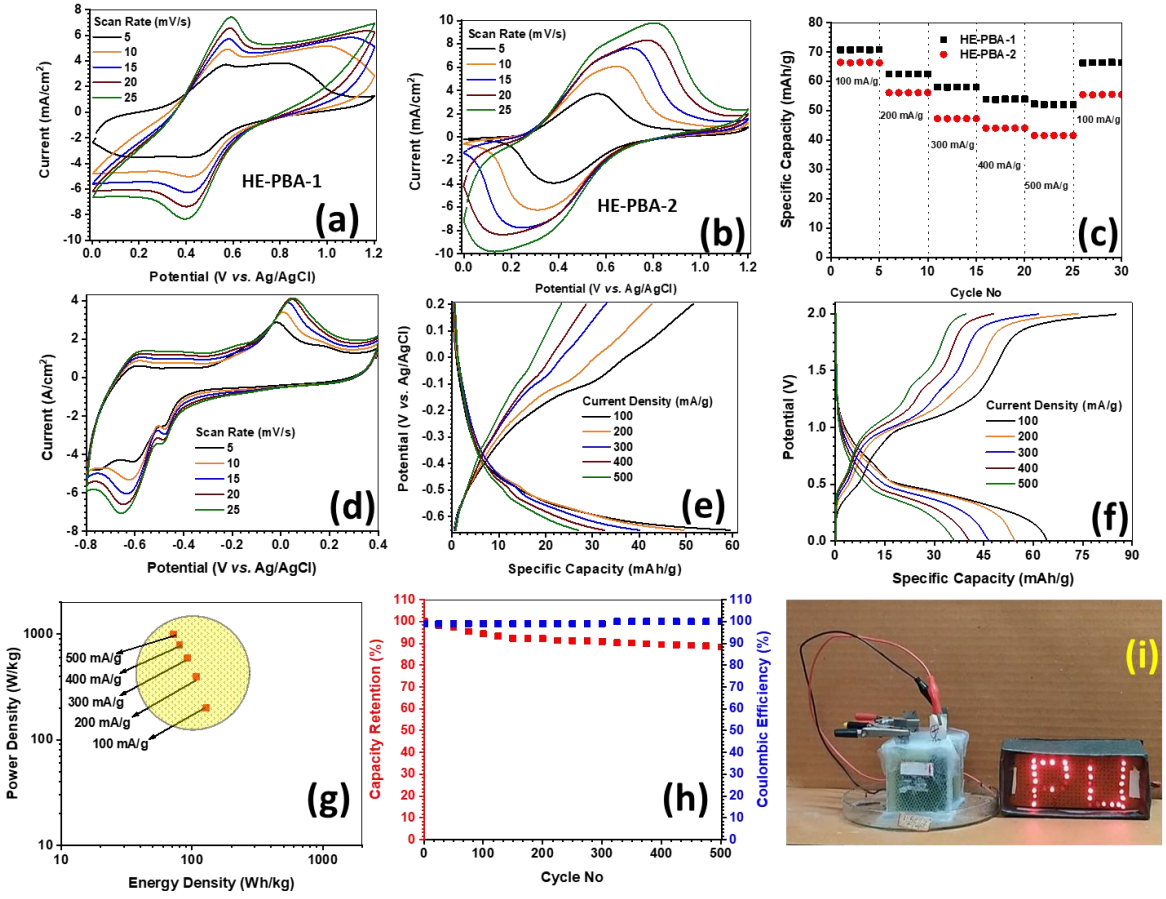

Figure 8: CV measurement at 5 to 25 mV/s scan rate within 0-1.2 V (a) HE-PBA-1, and (b) HE-PBA-2; (c) comparatively rate capability profile of HE-PBA-1 and HE-PBA-2; (d) CV profile of Cu-PBA derived oxide at 5 to 25 mV/s within 0.4 to -0.8 V *vs.* Ag/AgCl; (e) GCD profile of PBA-derived oxide at 100 to 500 mA/g within 0.2 to -0.7 V *vs.*Ag/AgCl; (f) GCD profile of 2 V cell configure with HE-PBA-1//PBA-derived oxide in CMC-SiO_2-1 M Na_2SO_4 gel; (g) Ragone plot: energy and power density at different current density; (h) Cycling profile of 2 V cells over 300 cycles at 200 mA/g current density; (i) 4 V device illuminating 3 V/270 mW LED setup.

Conclusions

It is evident from the electrochemical analysis that among two different HE-PBAs, HE-PBA-1 demonstrates better energy storage performance compared to HE-PBA-2 as a positive material for aqueous Na ion batteries. PBA-derived oxide also shows prominent electrochemical characteristics as a negative material. The resulting full cell demonstrates appreciable battery performances for solar energy storage.

References:

1. K. Hurlbutt, S. Wheeler, I. Capone and M. Pasta, *Joule*, 2018, **2**, 1950-1960.
2. G. Du and H. Pang, *Energy Storage Mater.*, 2021, **36**, 387-408.
3. P. Naskar, D. Kundu, A. Maiti, P. Chakraborty, B. Biswas and A. Banerjee, *ChemElectroChem*, 2021, **8**, 1393-1429.
4. J. Chen, L. Wei, A. Mahmood, Z. Pei, Z. Zhou, X. Chen and Y. Chen, *Energy Storage Mater.*, 2020, **25**, 585-612.

List of Publications

Research Articles:

1. P. Naskar, S. Mondal, B. Biswas, S. Laha and A. Banerjee, *J. Electrochem. Soc.*, 2023, **170**, 090535. (Impact Factor 3.9)
2. P. Naskar, S. Debnath, B. Biswas, S. Laha and A. Banerjee, *ACS Appl.EnergyMater.*, 2023, **6**, 4604-4617. (Impact Factor 6.4)
3. P. Naskar, S. Mondal, B. Biswas, S. Laha and A Banerjee, *Sustainable Energy &* Fuels, 2023, **7**, 4189-4201. (Impact Factor 6.8)
4. P. Naskar, S. Debnath, A. Maiti, B. Biswas and A. Banerjee, *ChemPhysChem*, 2023, **24**, e202200588. (Cover Feature) (Impact Factor 3.5)

Review Articles:

1. P. Naskar, A. Saha, B. Biswas and A. Banerjee, *J. Electrochem. Soc.*, 2024, doi.org/10.1149/1945-7111/ad1c16. (Impact Factor 3.9)
2. P. Naskar, S. Debnath, N. Mukherjee and A. Banerjee, *Resonance*, 2023, **28**, 577-596. (Impact Factor 0.5)
3. P. Naskar, D. Kundu, A. Maiti, P. Chakraborty, B. Biswas and A. Banerjee, *ChemElectroChem*, 2021, **8**, 1390-1390. (Cover Feature) (Impact Factor 4.7)
4. P. Naskar, P. Chakraborty, D. Kundu, A. Maiti, B. Biswas and A. Banerjee, *ChemistrySelect*, 2021, **6**, 1127-1161. (Impact Factor 2.3)
5. P. Naskar, A. Maiti, P. Chakraborty, D. Kundu, B. Biswas and A. Banerjee, *J. Mater. Chem. A*, 2021, **9**, 1970-2017. (Impact Factor 11.9)
6. S. Debnath, A. Maiti, P. Naskar, A Banerjee, *ChemNanoMat*., 2022, **8**, e202200261. (Impact Factor 3.8)

Patent

1. Aqueous Energy Storage Device, A. Banerjee, P. Naskar, S. Debnath and A. Maiti, Indian Patent Application No: 202231010840; filed on 28.02.2022. Publication Date (U/S11A):01.09.2023

Paper presented in National / International Symposium / Conferences

1. One Day International Seminar "Innovation, Expansion, Impact and Challenges in Chemical and Biological Science-2024", Department of Chemistry & IQAC, Surendranath College, 24/2 M. G. Road, Kolkata-70009 (Poster Presentation)
2. P. C. Ray Memorial International Conference on 'Contemporary Ideas, Innovations & Initiatives in Chemical Science CI3CS-2023', Department of Chemistry, Presidency University, Kolkata (Poster Presentation)
3. One Day National Symposium on 'FRONTIER IN CHEMISTRY: FROM FUNDAMENTALS TO APPLICATION', Department of Chemistry, Presidency University, Kolkata (Poster Presentation)
4. 29th CRSI-NATIONAL SYMPOSIUM IN CHEMISTRY & CRSI-ACS SYMPOSIUM SERIES IN CHEMISTRY 2022, IISER MOHALI (Poster Presentation)